Preclinical Characterization of a Novel Class of ^{18}F-Labeled PET Tracers for Amyloid-β

Damian Brockschnieder[1], Heribert Schmitt-Willich[1], Tobias Heinrich[1], Andrea Varrone[2], Balázs Gulyás[2], Miklos Toth[2], Jan Andersson[2], Ulf Boemer[1], Sabine Krause[1], Matthias Friebe[3], Ludger Dinkelborg[3], Christer Halldin[2], and Thomas Dyrks[1]

[1]Bayer HealthCare, Global Drug Discovery, Berlin, Germany; [2]Department of Clinical Neuroscience, Karolinska Institutet, Stockholm, Sweden; and [3]Piramal Imaging GmbH, Berlin, Germany

Imaging of amyloid-β (Aβ) plaques by PET is more and more integrated into concepts for Alzheimer disease (AD) diagnosis and drug development. The objective of this study was to find novel chemical entities that can be transformed into ^{18}F-labeled Aβ tracers with favorable brain washout kinetics and low background signal. **Methods:** High-throughput screening of a large chemical library was used to identify new ligands for fibrillar aggregates of $A\beta_{1-42}$ peptide. Thirty-two fluorinated derivatives were synthesized and tested for their affinity toward AD brain homogenate. Twelve ligands have been radiolabeled with ^{18}F. The pharmacokinetic properties of the radioligands were investigated in mouse and monkey biodistribution studies. Binding characteristics were determined by autoradiography of AD brain sections in vitro and using amyloid precursor protein transgenic mice in vivo. **Results:** The systematic search for Aβ imaging agents revealed several fluorinated derivatives with nanomolar affinity for Aβ. The fluoropyridyl derivative BAY 1008472 showed a high initial brain uptake (6.45 percentage injected dose per gram at 2 min) and rapid brain washout (ratio of percentage of injected dose per gram of tissue at 2 and 30 min after injection, 9.2) in mice. PET studies of healthy rhesus monkeys confirmed the high initial brain uptake of BAY 1008472 (2.52 standardized uptake value at peak) and a fast elimination of total radioactivity from gray and white matter areas (ratio of standardized uptake value at peak uptake and 60 min 11.0). In autoradiographic analysis, BAY 1008472 selectively detected Aβ deposits in human AD brain sections with high contrast and did not bind to τ- or α-synuclein pathologies. Finally, ex vivo autoradiography of brain sections from amyloid precursor protein-transgenic mice confirmed that BAY 1008472 is indeed suitable for the in vivo detection of Aβ plaques. **Conclusion:** A new chemical class of Aβ tracers has been identified by high-throughput screening. The fluoropyridyl derivative BAY 1008472 shows a favorable preclinical profile including low background binding in gray and white matter. These properties might qualify this new tracer, in particular, to detect subtle amounts or changes of Aβ burden in presymptomatic AD and during therapy.

Key Words: amyloid beta; PET imaging; Alzheimer's disease; dementia diagnosis

J Nucl Med 2012; 53:1794–1801
DOI: 10.2967/jnumed.112.104810

According to the amyloid hypothesis, aggregated amyloid-β (Aβ) peptides have a primary role in the etiology of Alzheimer disease (AD) (*1*). Plaques consisting of Aβ can be found in brain parenchyma, probably years before the onset of clinical symptoms (*2*). The Aβ peptide is released from the amyloid precursor protein by subsequent proteolytic cleavage of γ- and β-secretases. It aggregates into oligomeric and fibrillar structures of different sizes. Aβ can be detected postmortem in brain sections by immunostaining or histologic dyes such as Congo red or thioflavin T (*3*).

The definitive diagnosis of AD still depends on neuropathologic assessments after brain autopsy. Currently accepted pathologic criteria for AD include the verification of abnormal levels of Aβ plaques in the brain, and the absence of this pathologic marker is sufficient to rule out AD (*4,5*). Therefore, noninvasive techniques that allow the precise measurement of Aβ during a lifetime would be of great clinical value. There have been recent advances in cerebrospinal fluid analysis showing that the concentration of Aβ peptides is probably inversely correlated to the presence of Aβ plaques in the brain (*6–8*). With imaging techniques, such as PET, a direct visualization of the concentration and localization of amyloid deposits throughout the brain has become possible (*9*).

The first and most widely used PET tracer is ^{11}C-Pittsburgh compound B, which binds to fibrillar Aβ and shows a specific uptake in the brains of AD patients versus controls (*10*). The major disadvantage for a widespread clinical application of ^{11}C-Pittsburgh compound B PET is the short half-life of ^{11}C (20 min), limiting its use to PET centers with an onsite cyclotron and radiochemistry expertise. Therefore, ^{18}F-labeled radiotracers with a longer half-life (110 min), such as ^{18}F-florbetaben, ^{18}F-florbetapir, and ^{18}F-flutemetamol, have been designed and are currently in late-stage development (*11–13*).

Received Feb. 20, 2012; revision accepted Jun. 18, 2012.
For correspondence or reprints contact: Thomas Dyrks, Bayer Healthcare, Global Drug Discovery, Spiessweg 90, 13437 Berlin, Germany.
E-mail: Thomas.dyrks@bayer.com
Published online Sep. 24, 2012.

PET studies with ^{18}F-florbetaben, for example, have demonstrated widespread neocortical binding in patients diagnosed with AD, mild cognitive impairment, and other neurodegenerative conditions such as dementia with Lewy bodies (*9,14*). The success of early detection of Aβ in the disease process has spurred a major revision of the diagnostic criteria of AD toward the integration of Aβ as a biomarker for AD. The inclusion of biomarkers is expected to lead to an earlier and more accurate diagnosis of dementias (*15,16*).

There is a continuous quest to develop imaging probes with favorable brain disposition features and the highest detection sensitivity and optimal image quality (*17,18*). The nonspecific binding in the brain, especially, is a parameter that should be minimized, because in situations with low plaque load (e.g., in low-density regions or in prodromal AD) spillover effects of radioactivity, particularly from white matter, can affect the accurate assessment of Aβ in adjacent cortical regions. Despite these challenges, the chemical space that was investigated to find Aβ probes has for the most part been limited to variations of historical dyes used in neuropathology (*19,20*). We describe here the preclinical characterization of a novel chemical entity that was found through unbiased high-throughput screening of a large chemical library. The objective of the current study was to find novel Aβ tracers with favorable brain washout kinetics and low background signal.

MATERIALS AND METHODS

Chemical Synthesis of ^{19}F and ^{3}H Substances

The synthesis of compounds **1**–**12** is described in the supplemental information (supplemental materials are available online only at http://jnm.snmjournals.org) and Patent Cooperation Treaty international patent application WO 2010/028776 (published March 18, 2010 (*21*)).

^{3}H-**1** (*N*-(2-{4-[5-(benzyloxy)pyridine-2-yl][2,6-^{3}H]piperazin-1-yl}-2-oxoethyl)-2-fluoroisonicotinamide) was synthesized by a 1-pot isotope-exchange reaction using **1**, tritium gas and (1,5-cyclooctadien)-bis-(methyldiphenylphosphine)-iridium(I)-hexafluorophosphate as a catalyst (*22*). The degree of labeling was determined by liquid chromatography–mass spectrometry. The distribution of tritium in the labeled molecules corresponds to a specific activity of 3.75 TBq/mmol. More than 60% of the molecules contained 4 tritium atoms, and more than 30% of the molecules contained 3 tritium atoms. The labeling positions were in the 2 and 6 position of the piperazine ring, which was determined by ^{3}H-nuclear magnetic resonance spectroscopy. No other signals were detected.

Radiosynthesis of ^{18}F-1 (BAY 1008472)

The radiolabeling of BAY 1008472 was accomplished by a nucleophilic ^{18}F-fluorination of the corresponding bromo- or iodo-precursor. Detailed results of the optimization of BAY 1008472 radiosynthesis can be found in the supplemental information. Descriptions of the radiosyntheses of the other compounds can be found in patent applications WO 2011/095593 (*23*) and WO 2010/028776 (*21*).

In Vitro Binding Assay

Brain homogenates were prepared by homogenizing (Ultra Turrax [IKA]; 24,000 rpm for 30 s) pieces of the frontal cortex from 3 AD patients (Braak stages 4–5) in phosphate-buffered saline (pH 7.4) at a concentration of 100 mg of wet tissue per milliliter. The human brain tissue used in this study was sourced and prepared by the Victorian Brain Bank Network (Australia) or by The Netherlands Brain Bank.

The homogenate was divided into aliquots of 300 μL and stored at −80°C. To determine the inhibitory concentration of 50% (IC_{50}), a competition assay using AD brain homogenate was performed in 96-well plates (Greiner Bio-One) as triplicates. Therefore, increasing concentrations of test substances (0.5 nM to 1 μM) were incubated with brain homogenate (100 μg of protein/mL), 10 nM tritiated Aβ ligand in phosphate-buffered saline, and 0.1% bovine serum albumin (final volume, 200 μL). After incubation for 3 h at room temperature, the reaction mixture was filtered through GF/B filters (Perkin Elmer) using a Filtermate 196 harvester (Packard). After that, filters were washed twice with phosphate-buffered saline and 0.1% bovine serum albumin. Then, 40 μL of liquid scintillator were added to each well, and the bound radioactivity was measured in a TopCount device (Perkin Elmer). Nonspecific binding was assessed by adding an excess of the unlabeled reference ligand to the reaction mixture. IC_{50} values were calculated by nonlinear regression analysis with the help of GraFit 5.0 software (Erithacus Software) and represent mean values of 3 measurements.

^{18}F Autoradiography and Tritium Emulsion Autoradiography

The autoradiography experiments were performed as recently described by Fodero-Tavoletti et al. (*24*). Specifically, sections were incubated with BAY 1008472 (10 Bq/μL), and for blocking experiments an excess of ^{19}F-**1** compound (10 μM) was added to the incubation mixture. For photoemulsion autoradiography, sections were incubated with 11 Bq/μL of ^{3}H-**1**.

Biodistribution of ^{18}F Substances and Ex Vivo Autoradiography Using Amyloid Precursor Protein Transgenic Mice

Biodistribution and excretion studies were performed in male NMRI mice (body weight, ~30 g; 3 animals per time point). The animals were kept under normal laboratory conditions. The animal studies were performed according to institutional guidelines and approved by the Berlin animal welfare authorities. At 2 min, 5 min, 30 min, 1 h, and 4 h after injection of about 185 kBq of test compound into the tail vein, urine and feces were quantitatively collected. At the same time points, animals were sacrificed by decapitation under isoflurane anesthesia, and organs and tissues of interest (spleen, liver, kidneys, lung, bone [femur], heart, brain, fat, thyroid, muscle, skin, blood, tail, stomach, testicle, intestine, pancreas, and adrenals) were removed for the determination of radioactivity using a γ-counter. The decay-corrected percentage of injected dose per tissue weight (%ID/g ± SD) was calculated.

For ex vivo autoradiography experiments, we used hemizygous Tg2576 transgenic mice (age, >20 mo; Taconic (*25*)). Approximately 10 MBq of BAY 1008472 were injected through the tail vein. The animals were killed by decapitation at 40 and 60 min after intravenous injection ($n = 3$). The brains were immediately removed and frozen on dry ice. Sections of 18 μm were cut on a cryostat and exposed to phosphoimaging plates.

PET in Rhesus Monkeys

Two female rhesus monkeys (weight, 3.5–4.8 kg) were used for each tracer. The study was approved by the Animal Ethics Committee of the Swedish Animal Welfare Agency (no. 260/07) and was performed according to the *Guidelines for Planning, Conducting and Documenting Experimental Research* (no. 4820/06-600) (*26*) of the Karolinska Institutet and the *Guide for the Care*

and Use of Laboratory Animals of the National Institutes of Health (*27*).

Anesthesia was induced by intramuscular injection of ketamine hydrochloride and maintained by the administration of a mixture of isoflurane (2%–8%), O_2, and medical air after endotracheal incubation. The head was immobilized with a fixation device. Body temperature was maintained by a Bair Hugger unit (model 505; Arizant Healthcare) and monitored by an esophageal thermometer. Electrocardiogram, heart rate, respiratory rate, and oxygen saturation were continuously monitored throughout the experiments. Blood pressure was monitored every 15 min (details of the procedure are provided in the study by Takano et al. (*28*)).

The PET scanner was an HRRT research tomograph (Siemens Molecular Imaging) with an in-plane spatial resolution (full width at half maximum) of 1.5 mm (*29*). A transmission scan of 6 min using a single ^{137}Cs source was performed immediately before the radioligand injection. List-mode data were acquired continuously for 123 min immediately after intravenous injection. Images were reconstructed with ordinary Poisson 3-dimensional ordered-subset expectation maximization using point spread function modeling, with a series of frames of increasing duration (9×20, 3×60, 5×180, and 17×360 s). For image quantification, time–activity curves of standardized uptake values (SUV, expressed in percentage), made for several regions of interest, were used. The regions of interest were as follows: thalamus, temporal cortex, frontal cortex, white matter (at the level of the centrum semiovale), cerebellum, and whole brain. Regions of interest were coregistered to MR images, with the help of an atlas of the rhesus monkey brain.

RESULTS

Affinity of Fluorinated Derivatives for Aβ

The novel *N,N′*-disubstituted piperazine scaffold was discovered by high-throughput screening of a large chemical library (>700,000 compounds) for ligands of synthetic $A\beta_{1-42}$ fibrils (D. Brockschnieder, unpublished data, 2011). Hits **H1–H3** (Fig. 1) are characterized by a scaffold based on *N*-acyl, *N′*-4-benzyloxyphenyl piperazine. These hits differ only in the acylated substituent of piperazine (west side of the molecule). As the initial hits carried no fluorine atom, we synthesized 32 derivatives with ^{19}F in a position accessible for radiolabeling. Using a radioactive competition assay to determine the affinity toward AD brain homogenate, we obtained a comprehensive structure–activity relationship (Table 1; Supplemental Fig. 1). Substances with IC_{50} values of less than 100 nM were considered as high-affinity ligands. Established reference ligands such as florbetaben showed affinities in a comparable range under identical assay conditions (Table 1).

More than thirty ^{19}F-containing compounds based on the *N*-acyl, *N′*-phenyl piperazine scaffold were synthesized to select the most potent candidates in terms of binding affinity toward AD brain homogenate (Fig. 1 and Supplemental Fig. 1 for compounds **13**–**32**). In general, variations in the west side of the molecule (*N*-acyl substituent of piperazine) are much more tolerated than variations in the east side, that is, changes in the 4-*O*-benzyl-phenyl residue. For example, incorporation of a nitrogen in the 2 or 3 position of the outer benzyl ring (east side) leads to a loss of affinity (**15, 17, 22,** and **25**; Supplemental Fig. 1), and incorporation of a nitrogen in the central phenylen residue is allowed only at 1 of the 2 possible positions (e.g., **1** and **24** with an IC_{50} value of 39 and >100 nM, respectively). Replacement of -OCH_2- between the central phenyl ring and the outer benzyl ether by -O-CO- ester bond or -NH-CO- amide bond leads to loss of binding in most cases (**26, 27,** and **28**). However, if the introduction of this amide bond is combined with a naphthyl residue (**10, 19,** and **20**), binding affinity might be restored. The outer benzyl ring at the east side is essential (**21**).

At the west side of the molecule, much larger changes seem to be tolerable (e.g., compounds **2**–**8, 14, 20,** and **32**). Interestingly, among the various fluoropyridyl–carboxylic acid amide isomers, 6-fluoro-pyridine-2-carboxylic acid amide **29** (>100 nM) has a much lower binding affinity than the structurally similar 2-fluoro-pyridine-4-carboxylic acid amide **2** (13 nM) and 2-fluoro-pyridine-3-carboxylic acid amide **5** (25 nM).

Biodistribution in Healthy Mice

Having identified several fluorinated compounds with high binding affinity, we selected 12 compounds to be examined as radioactive derivatives in mouse biodistribution studies (Table 1). For that reason, we generated suitable precursor molecules for each compound and established a radiolabeling procedure with ^{18}F. A suitable radiotracer for the brain should have a good penetration of the blood–brain barrier, that is, a high uptake after bolus injection (>2–4 %ID/g in mice) and low unspecific binding in brain areas without target protein (*30,31*). The washout from the brain was described as a ratio of the %ID/g at 2 and 30 min after injection. Because wild-type mice have no Aβ plaques, a fast washout indicated by a high 2- to 30-min ratio is desired. Here, we were aiming at ratios greater than 5 because we wanted to improve the unspecific background, compared with established tracers (*32,33*).

The radioactive compounds **1**–**8** all showed a good penetration of the blood–brain barrier, indicated by a high brain uptake at 2 min after injection (>4 %ID/g) (Table 1). Compounds **9**–**13** showed significantly lower levels of brain uptake and were therefore not pursued. We did not investigate the cause for their inefficient penetration of the blood–brain barrier in detail; however, potential reasons might be an inappropriate hydrophilicity or molecular weight and poor metabolic stability. Notably, the fluoropropyl derivatives BAY 1008472 and ^{18}F-**2** showed a high uptake and rapid elimination of radioactivity from the brain as indicated by 2- to 30-min ratios greater than 5.5 and low retention at 4 h after injection (<0.05 %ID/g). Moreover, these 2 compounds did not show any accumulation of radioactivity in bones (<0.17 %ID/g at 4 h), which is a known indicator for the generation of free ^{18}F due to defluorination of the compound. A high accumulation of radioactivity into the cranial bones can cause undesired signals, which complicate the quantification of specific signals during brain PET.

The foregoing studies in healthy mice demonstrate the general suitability of the newly discovered chemical

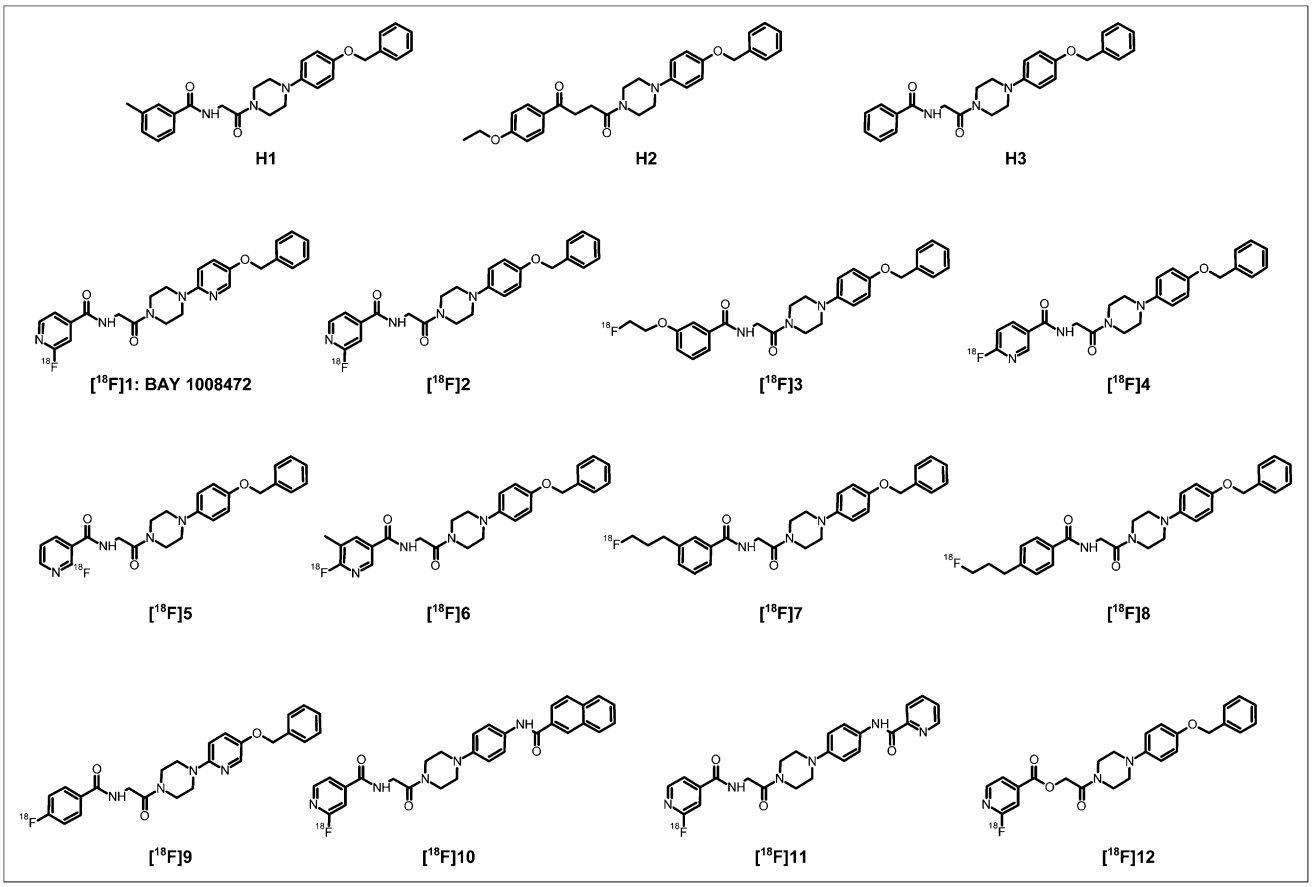

FIGURE 1. Structures of high-throughput screening hits (**H1**–**H3**) and ^{18}F-labeled compounds (**1**–**12**).

scaffold for brain imaging. The selected derivatives ^{18}F-**1** (BAY 1008472) and ^{18}F-**2** show higher brain uptake and faster washout than florbetaben and meet our stringent selection criteria for brain uptake and washout kinetics and were further investigated as candidates for successful Aβ imaging.

Monkey PET Studies

As a next step, we determined the kinetics of ^{18}F-**1** and ^{18}F-**2** (which differ only in the substitution of a phenylic carbon atom for nitrogen) in rhesus monkey brains by PET. Figure 2 illustrates a head-to-head comparison of both compounds in the same monkey. Almost identical results were obtained when

TABLE 1
Properties of Compounds Used in Biodistribution Experiments

Compound no.	IC_{50} (nM)	Brain uptake at 2 min (%ID/g)	Brain washout (ratio of percentage injected dose per gram of tissue at 2 and 30 min after injection)	Retention at 4 h (%ID/g)	Bone uptake at 4 h (%ID/g)
1 (BAY 1008472)	39	6.45	9.2	0.03	0.17
2	13	5.54	5.5	0.05	0.16
3	37	5.15	3.1	0.42	3.06
4	15	4.99	3.5	0.04	1.75
5	25	5.37	4.2	0.07	7.96
6	12	4.51	3.9	0.04	1.79
7	55	4.38	3.1	0.13	4.54
8	12	4.31	3.7	0.17	13.69
9	15	3.39	9.4	0.02	0.03
10	14	0.99	1.1	0.11	0.23
11	99	2.53	2.2	0.07	0.15
12	96	0.88	29.3	0.00	0.03
Florbetaben	44	4.77	3.0	0.95	4.64

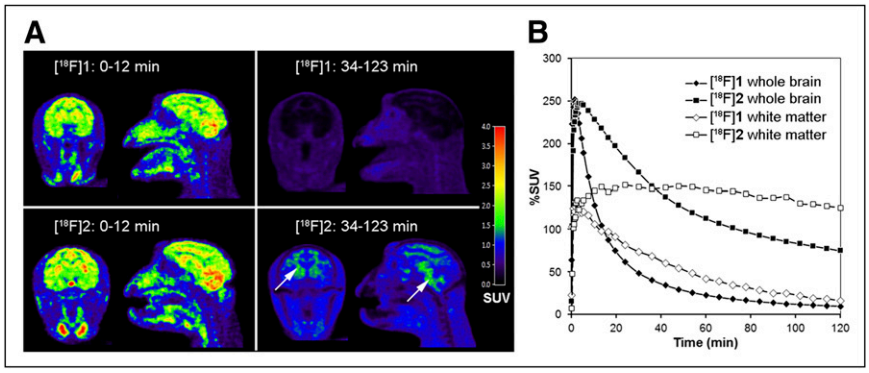

FIGURE 2. (A) Coronal and sagittal PET images of head after administration of BAY 1008472 and ^{18}F-2 to same monkey. Color coding depicts mean values of SUVs integrated over 0–12 min and 34–123 min after injection. BAY 1008472 shows faster clearance from brain and surrounding tissue than ^{18}F-2. White arrows point to white matter signals. (B) Time–activity curves for whole brain and white matter of same monkey as in A.

the 2 radioligands were administered to a different second monkey, confirming the head-to-head comparison. There was a high brain uptake for BAY 1008472 and ^{18}F-**2** (mean peak uptake for the 2 investigated monkeys, 252% and 255% SUV, respectively) and a relatively uniform distribution throughout the brain (Fig. 2A). As in mice, the compounds seemed resistant toward defluorination, because there was no obvious accumulation of radioactivity in the skull. Whole-brain time–activity curves demonstrated a significantly faster washout for BAY 1008472 than for ^{18}F-**2** and florbetaben (Fig. 2B; Supplemental Fig. 2) and a lower retention at later time points (>30 min), indicating less nonspecific binding. Besides the faster washout from all brain areas examined (thalamus, temporal cortex, frontal cortex, and cerebellum), BAY 1008472 showed also a much lower retention in myelin-rich white matter regions (Fig. 2). This lower retention might be an advantage over current PET tracers in development, because they all show a relatively high white matter background. The fast kinetics observed will also be a prerequisite for an early and prolonged imaging window with stable SUV ratios between target and reference region in a clinical setting.

Plasma analysis for radioactive metabolites of BAY 1008472 revealed only a polar metabolite fraction (Supplemental Fig. 3). On the basis of the fast brain washout and the absence of lipophilic metabolites (which could penetrate the blood–brain barrier), we assume that the metabolic profile of BAY 1008472 is supportive of rather than prohibitive for high-contrast imaging of Aβ.

Taken together, the monkey study confirms the fast washout kinetics in a higher species and identifies BAY 1008472 as the preferred substance.

In Situ and In Vivo Binding Properties of BAY 1008472

To further investigate whether BAY 1008472 (^{18}F-**1**) is suitable for the detection of Aβ deposits, we performed a detailed autoradiographic analysis. For this, we used well-characterized postmortem human brain tissue and additionally confirmed in serial sections the presence or absence of different pathologies by immunohistochemistry for Aβ- (1E8), τ- (AT8), and α-synuclein (LB509). In this immunohistochemistry analysis, the AD tissues showed frequent plaques in cortical areas mixed with τ-pathology and the absence of Lewy bodies. Frontotemporal dementia (FTD) tissues comprised only neurofibrillary tangle pathology.

As a first step, we investigated the binding pattern of BAY 1008472 to brain sections from AD and FTD patients and healthy controls (Fig. 3). The autoradiograms showed frequent plaquelike signals in cortical gray matter regions of AD tissue sections. Similar signals were also observed in white matter regions, albeit at much lower densities. The radioactive signal pattern matched well with subsequent immunohistochemical detection of Aβ plaques using the same sections. In contrast, in tissue sections from healthy controls and FTD subjects devoid of Aβ deposits, no plaquelike radioactive signals were observed. Furthermore, the signals in AD tissue could be blocked to a large extent with

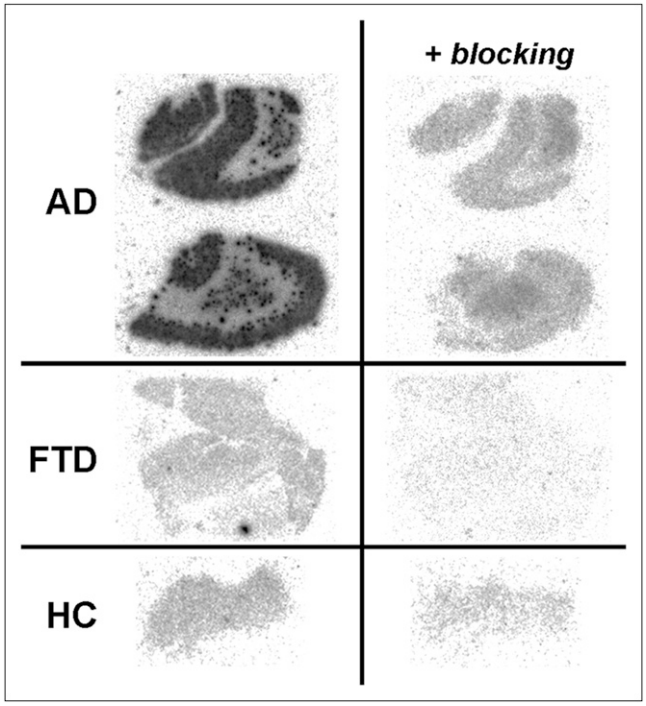

FIGURE 3. Autoradiographic analysis of binding of BAY 1008472 to brain sections from frontal cortex of 2 AD patients with Aβ plaques. Control sections devoid of Aβ pathology stem from healthy volunteer (HC) and FTD patient. Blocking of specific signals was performed with excess of cold BAY 1008472 compound (10 μM).

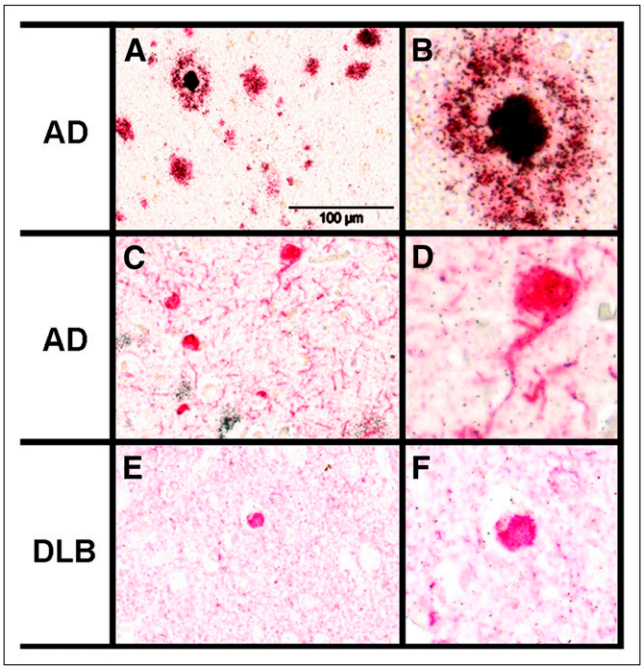

FIGURE 4. Photoemulsion autoradiographic analysis of binding of compound ^{3}H-**1** to brain sections from frontal cortex of AD (A–D) and dementia with Lewy bodies (DLB) (E and F) patients in combination with immunohistochemistry. (A) ^{3}H-**1** binding and Aβ immunohistochemistry (1E8). (B) Magnified image detail of A. (C) ^{3}H-**1** binding and paired helical filament immunohistochemistry (AT8). (D) Magnified image detail of C. (E) ^{3}H-**1** binding and α-synuclein immunohistochemistry (LB509). (F) Magnified image detail of E. Specific binding of ^{3}H-**1** is reflected by accumulation of silver grains. Immunopositive structures are stained red. Scale bar in A, C, and E is 100 µm.

an excess of the cold ^{19}F analog of BAY 1008472, confirming the specific mode of BAY 1008472 binding.

To further investigate the selectivity with respect to other amyloidogenic proteins, we developed a protocol that allowed us to study in parallel (on the same tissue section) compound binding, as detected by high-resolution photoemulsion autoradiography, and the localization of Aβ- , τ-, and α-synuclein aggregates, which were detected by immunohistochemistry. Because of the incompatibility of photoemulsion autoradiography with ^{18}F labels, this method required the use of a tritium-labeled analog of BAY 1008472 (^{3}H-**1**).

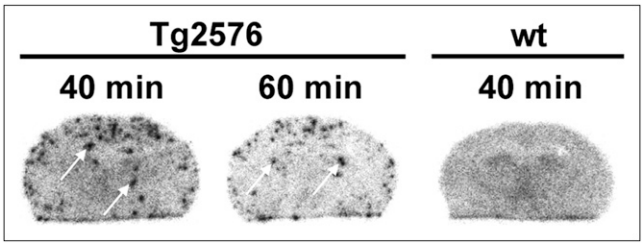

FIGURE 5. Ex vivo autoradiography of coronal brain sections after administration of BAY 1008472 to wild-type (wt) and Tg2576 transgenic mice. Mice were sacrificed at 40 or 60 min after tracer injection. White arrows point to plaque-specific signals.

Microscopic evaluation of emulsion-dipped, ^{3}H-**1**–treated AD brain sections with confirmed Aβ- and τ-pathologies revealed clustering of silver grains (representing ^{3}H-**1** signals) exclusively on 1E8 immunoreactive Aβ plaques (Figs. 4A and 4B). In general, the anti-Aβ antibody and the ^{3}H-**1** labeled identical structures in the tissue sections, with the highest densities of silver grains found in the center of cored plaques (Fig. 4B). There was no accumulation of silver grains above background levels on AT8 immunoreactive neurofibrillary tangles and neuropil threads (Figs. 4C and 4D). The binding of ^{3}H-**1** to α-synuclein deposits was investigated using brain sections exhibiting Lewy bodies. As for neurofibrillary tangles, there was no clustering of silver grains above background levels in association with α-synuclein immunoreactive Lewy bodies (Figs. 4E and 4F), indicating that ^{3}H-**1** has a high selectivity for Aβ pathology.

Finally, we tested whether BAY 1008472 is indeed able to detect Aβ plaques under in vivo conditions. Therefore, we used Tg2576 mice that overexpress amyloid precursor protein with Swedish mutation under control of the hamster prion promoter and that develop plaques after 8 mo of age (*25*). We injected BAY 1008472 into transgenic and wild-type animals more than 20 mo old and performed ex vivo autoradiography with brain sections at 40 and 60 min after injection. In sharp contrast to wild-type animals, autoradiograms of transgenic animals clearly showed numerous plaquelike signals up to 1 h after injection, indicating an efficient and stable labeling of plaques over the whole observation period (Fig. 5). The presence or absence of plaques was independently confirmed by subsequent histochemistry using the same sections.

The foregoing set of experiments proves that BAY 1008472 is able to detect amyloid plaques in vivo.

DISCUSSION

This study describes, to our knowledge, the first systematic high-throughput screen of a large chemical library aiming at the development of PET tracers. It demonstrates not only that classic receptors harboring a single binding pocket but also that fibrillar aggregates of Aβ with structurally less defined binding characteristics (*3,34*) can be suitable targets for a high-throughput screening approach. This finding is of relevance for the development of PET tracers for τ- or α-synuclein deposits because these proteins also have an amyloidogenic character and form filamentous structures under disease conditions. The availability of imaging probes for τ-PHFs or α-synuclein deposits would significantly enlarge the diagnostic methods for the detection of brain pathologies and will support differential diagnosis and staging of dementias as well as the development of pathology-targeted therapies (*35–37*).

The tracers described herein belong to a novel class of Aβ ligands that is structurally not related to previous ligands (i.e., mostly benzothiazoles and stilbenes). The most potent compound, BAY 1008472, was found through an extensive lead-finding program involving the synthesis of more than 30 cold compounds and investigation of twelve ^{18}F derivatives in in

vivo experiments. In our lead-finding program, we observed that subtle changes of substituents not only affected binding affinity in a structure–activity relationship but strongly influenced pharmacokinetic parameters. These effects may be related to changes in physicochemical properties such as lipophilicity or metabolic degradation.

An ideal PET tracer for Aβ would have negligible nonspecific binding in white and gray matter combined with an early equilibrium and fast washout after injection of the tracer (*31*). These properties are the basis for a high sensitivity and flexible imaging window in clinical use. The newly discovered compound BAY 1008472 shows in this respect an excellent preclinical profile: it binds with nanomolar target affinity, analogously to established Aβ tracers. It readily enters the brain in high amounts after bolus injection and is rapidly eliminated from brain tissue devoid of plaques. Importantly, monkey imaging studies demonstrated a remarkably low retention in white matter regions. In autoradiographic analysis, BAY 1008472 selectively binds to Aβ plaques in human brain tissue. High-resolution photoemulsion autoradiography revealed that there was no binding to τ- and α-synuclein pathologies. This can be critical to avoid misinterpretation of the PET results, because these pathologies also comprise β-pleated sheet structures and frequently localize to similar brain regions (*38*). Finally, BAY 1008472 specifically and persistently labeled amyloid plaques of Tg2576 transgenic mice with good contrast in vivo. Besides these properties, for a clinical PET tracer with widespread application, an efficient radiolabeling procedure and in vitro stability would be additional prerequisites. By testing different precursor molecules and synthesis protocols we have found an effective and adequate process for BAY 1008472, yielding high amounts (>10 GBq) and high specific radioactivities (>130 GBq/μmol) without any signs of radiolysis.

Taking all preclinical parameters into consideration, we think that BAY 1008472 is a good candidate to be tested as a representative of a new chemical class of Aβ agents in a human proof-of-mechanism study. Such a study should initially involve a limited number of AD patients and healthy controls in order to get a first impression of its clinical potential. It is expected that an increased target-to-background ratio would provide better image quality in humans and higher sensitivity to detect low amounts of Aβ deposits in preclinical AD. Furthermore, high detection sensitivity will also support the development of therapies targeting Aβ by improving patient selection and the fidelity of monitoring changes in plaque burden over time.

CONCLUSION

We have identified a new chemical class of Aβ tracers by high-throughput screening. The fluoropyridyl derivative BAY 1008472 shows a favorable preclinical profile, including low background binding in gray and white matter. These properties might be particularly advantageous to detect low amounts or small changes of Aβ burden in early AD and during therapy.

DISCLOSURE STATEMENT

The costs of publication of this article were defrayed in part by the payment of page charges. Therefore, and solely to indicate this fact, this article is hereby marked "advertisement" in accordance with 18 USC section 1734.

ACKNOWLEDGMENTS

We thank all members of the project team for their constant support and Ulrich Pleiss for the supply of tritiated compounds. For excellent technical support, we are very grateful to Jana Hannig, Claudia Kamfenkel, Gül Caglar, Manuela Brand, Claudia Günther, Werner Behrendt, and Lorenz Behringer. No potential conflict of interest relevant to this article was reported.

REFERENCES

1. Hardy J, Selkoe DJ. The amyloid hypothesis of Alzheimer's disease: progress and problems on the road to therapeutics. *Science.* 2002;297:353–356.
2. Gelosa G, Brooks DJ. The prognostic value of amyloid imaging. *Eur J Nucl Med Mol Imaging.* 2012;39:1207–1219.
3. Reinke AA, Gestwicki JE. Insight into amyloid structure using chemical probes. *Chem Biol Drug Des.* 2011;77:399–411.
4. Mirra SS, Heyman A, McKeel D, et al. The Consortium to Establish a Registry for Alzheimer's Disease (CERAD). Part II: standardization of the neuropathologic assessment of Alzheimer's disease. *Neurology.* 1991;41:479–486.
5. Hyman BT, Trojanowski JQ. Consensus recommendations for the postmortem diagnosis of Alzheimer disease from the National Institute on Aging and the Reagan Institute Working Group on diagnostic criteria for the neuropathological assessment of Alzheimer disease. *J Neuropathol Exp Neurol.* 1997;56:1095–1097.
6. Fagan AM, Mintun MA, Mach RH, et al. Inverse relation between in vivo amyloid imaging load and cerebrospinal fluid Abeta42 in humans. *Ann Neurol.* 2006;59:512–519.
7. Trojanowski JQ, Vandeerstichele H, Korecka M, et al. Update on the biomarker core of the Alzheimer's Disease Neuroimaging Initiative subjects. *Alzheimers Dement.* 2010;6:230–238.
8. De Meyer G, Shapiro F, Vanderstichele H, et al. Diagnosis-independent Alzheimer disease biomarker signature in cognitively normal elderly people. *Arch Neurol.* 2010;67:949–956.
9. Villemagne VL, Ong K, Mulligan RS, et al. Amyloid imaging with ^{18}F-florbetaben in Alzheimer disease and other dementias. *J Nucl Med.* 2011;52:1210–1217.
10. Klunk WE, Engler H, Nordberg A, et al. Imaging brain amyloid in Alzheimer's disease with Pittsburgh Compound-B. *Ann Neurol.* 2004;55:306–319.
11. Rowe CC, Ackerman U, Browne W, et al. Imaging of amyloid beta in Alzheimer's disease with ^{18}F-BAY94-9172, a novel PET tracer: proof of mechanism. *Lancet Neurol.* 2008;7:129–135.
12. Wong DF, Rosenberg PB, Zhou Y, et al. In vivo imaging of amyloid deposition in Alzheimer disease using the radioligand ^{18}F-AV-45 (florbetapir [corrected] F 18). *J Nucl Med.* 2010;51:913–920.
13. Vandenberghe R, Van Laere K, Ivanoiu A, et al. ^{18}F-flutemetamol amyloid imaging in Alzheimer disease and mild cognitive impairment: a phase 2 trial. *Ann Neurol.* 2010;68:319–329.
14. Barthel H, Gertz HJ, Dresel S, et al. Cerebral amyloid-beta PET with florbetaben (^{18}F) in patients with Alzheimer's disease and healthy controls: a multicentre phase 2 diagnostic study. *Lancet Neurol.* 2011;10:424–435.
15. Dubois B, Feldman HH, Jacova C, et al. Revising the definition of Alzheimer's disease: a new lexicon. *Lancet Neurol.* 2010;9:1118–1127.
16. Jack CR Jr, Albert MS, Knopman DS, et al. Introduction to the recommendations from the National Institute on Aging-Alzheimer's Association workgroups on diagnostic guidelines for Alzheimer's disease. *Alzheimers Dement.* 2011;7:257–262.
17. Ono M. Development of positron-emission tomography/single-photon emission computed tomography imaging probes for in vivo detection of beta-amyloid plaques in Alzheimer's brains. *Chem Pharm Bull (Tokyo).* 2009;57:1029–1039.
18. Juréus A, Swahn BM, Sandell J, et al. Characterization of AZD4694, a novel fluorinated Abeta plaque neuroimaging PET radioligand. *J Neurochem.* 2010; 114:784–794.
19. Kung HF, Choi SR, Qu W, Zhang W, Skovronsky D. ^{18}F stilbenes and styrylpyridines for PET imaging of A beta plaques in Alzheimer's disease: a miniperspective. *J Med Chem.* 2010;53:933–941.

20. Klunk WE, Debnath ML, Pettegrew JW. Development of small molecule probes for the beta-amyloid protein of Alzheimer's disease. *Neurobiol Aging.* 1994;15: 691–698.
21. Schmitt-Willich H, Roehn U, Friebe M, et al. Preparation of isotope-labeled piperazine derivatives for binding and imaging amyloid plaques and their use. PCT International Application WO 2010028776 A1 20100318. 2010.
22. Pleiss U. Synthesis of [^{3}H] vardenafil, Levitra, using a new labeling technique. *J Labelled Comp Radiopharm.* 2003;46:1241–1247.
23. Schmitt-Willich H, Heinrich T, Brockschnieder D. Process for preparation of 18F-labeled piperazine derivative as PET imaging agent of amyloid plaques. PCT International Application WO 2011095593. 2011.
24. Fodero-Tavoletti MT, Brockschnieder D, Villemagne VL, et al. In vitro characterization of [^{18}F]-florbetaben, an Abeta imaging radiotracer. *Nucl Med Biol.* April 11, 2012 [Epub ahead of print].
25. Hsiao K, Chapman P, Nilsen S, et al. Correlative memory deficits, Abeta elevation, and amyloid plaques in transgenic mice. *Science.* 1996;274:99–102.
26. *Guidelines for Planning, Conducting and Documenting Experimental Research*. Available from: http://ki.se/content/1/c6/09/78/88/experimentell_en.pdf. Accessed August 24, 2012.
27. *Guide for the Care and Use of Laboratory Animals*. Bethesda, MD: National Institutes of Health; 1985. NIH publication 85–23.
28. Takano A, Gulyas B, Varrone A, Maguire RP, Halldin C. Saturated norepinephrine transporter occupancy by atomoxetine relevant to clinical doses: a rhesus monkey study with (S,S)-[^{18}F]FMeNER-D (2). *Eur J Nucl Med Mol Imaging.* 2009;36:1308–1314.
29. Varrone A, Sjoholm N, Eriksson L, Gulyas B, Halldin C, Farde L. Advancement in PET quantification using 3D-OP-OSEM point spread function reconstruction with the HRRT. *Eur J Nucl Med Mol Imaging.* 2009;36:1639–1650.
30. Halldin C, Gulyas B, Langer O, Farde L. Brain radioligands: state of the art and new trends. *Q J Nucl Med.* 2001;45:139–152.
31. Laruelle M, Slifstein M, Huang Y. Relationships between radiotracer properties and image quality in molecular imaging of the brain with positron emission tomography. *Mol Imaging Biol.* 2003;5:363–375.
32. Zhang W, Oya S, Kung MP, Hou C, Maier DL, Kung HF. F-18 stilbenes as PET imaging agents for detecting beta-amyloid plaques in the brain. *J Med Chem.* 2005;48:5980–5988.
33. Choi SR, Golding G, Zhuang Z, et al. Preclinical properties of ^{18}F-AV-45: a PET agent for Abeta plaques in the brain. *J Nucl Med.* 2009;50:1887–1894.
34. LeVine H 3rd. Multiple ligand binding sites on A beta(1-40) fibrils. *Amyloid.* 2005;12:5–14.
35. Vernon AC, Ballard C, Modo M. Neuroimaging for Lewy body disease: is the in vivo molecular imaging of alpha-synuclein neuropathology required and feasible? *Brain Res Rev.* 2010;65:28–55.
36. Rinne JO, Brooks DJ, Rossor MN, et al. ^{11}C-PiB PET assessment of change in fibrillar amyloid-beta load in patients with Alzheimer's disease treated with bapineuzumab: a phase 2, double-blind, placebo-controlled, ascending-dose study. *Lancet Neurol.* 2010;9:363–372.
37. Berti V, Pupi A, Mosconi L. PET/CT in diagnosis of dementia. *Ann N Y Acad Sci.* 2011;1228:81–92.
38. Jellinger KA. Basic mechanisms of neurodegeneration: a critical update. *J Cell Mol Med.* 2010;14:457–487.